Electromagnetics, 31:355–367, 2011

ISSN: 0272-6343 print/1532-527X online
DOI: 10.1080/02726343.2011.579770

Pattern Synthesis with Specified Broad Nulls in Time-Modulated Circular Antenna Arrays

LI ZHENG,[1] SHIWEN YANG,[1] and ZAIPING NIE[1]

[1]Department of Microwave Engineering, School of Electronic Engineering, University of Electronic Science and Technology of China, Chengdu, P. R. China

Abstract *This article presents an approach for the synthesis of time-modulated circular array patterns with specified null width constraints. The time-modulated circular antenna arrays with uniform amplitude excitations are designed through the differential evolution algorithm with their excitation phases, and the switch-on time intervals of each element of the time-modulated circular arrays are the variables to be optimized. Several examples synthesized from the time-modulated circular array with the prescribed null width and depth are compared with some published results of the conventional circular array. Simulation results illustrate the achievable performance of the approach in successfully synthesizing patterns with desirable broad nulls, even if the amplitude excitations are uniform.*

Keywords circular arrays, wide nulls, time modulation, differential evolution

1. Introduction

The use of a null adjustable position in the radiation pattern of a receiving antenna array is often suggested as a means of "eliminating" an interfering signal, thus improving the quality of reception of the wanted signal (Gething & Haseler, 1974). Antenna arrays with low side-lobe radiation patterns cannot guarantee good reception of the desirable signal in the presence of strongly polluted electromagnetic environments. In order to reject interference signals, it is often necessary to place deep nulls in the pattern. However, in the case that the interference signals are incident from several different directions or variable slightly with time, the positions of the pattern nulls have to be continuously adjustable. In order to avoid the inconvenience of continuous null steering, a relatively wide null on the mean directions of arrival of the interference signals is desirable. Thus, there has been considerable interest in the synthesis of antenna array patterns with prescribed broad nulls (Giusto & De Vincenti, 1983; Er, 1988, 1990; Guney & Onay, 2007; Lu & Yeo, 2000; Karaminas & Minikas, 2000; Gome-Tomero et al., 2010). However, most of these studies were on the linear arrays, and to the best knowledge of the authors, studies were rarely conducted on the synthesis of antenna patterns with broad nulls in circular arrays, especially in recent years.

Received 15 November 2010; accepted 23 March 2011.
Address correspondence to Shiwen Yang, Department of Microwave Engineering, School of Electronic Engineering, University of Electronic Science and Technology of China (UESTC), Chengdu, 610054, P. R. China. E-mail: swnyang@uestc.edu.cn

On the other hand, in recent years, the time-modulation technique has been widely used to synthesize low/ultra-low side-lobes (Kummer et al., 1963; Yang et al., 2003, 2004b, 2005, 2009; Rocca et al., 2009, 2010). With the additional degree of design freedom—time—the dynamic-range ratio of the excitation can be significantly reduced. As for the time parameter, it can be adjusted easily, rapidly, and accurately; the stringent requirements on various error tolerances can also be relaxed. However, the inherent drawback of the time-modulated arrays is that there are many sideband signals spaced at multiples of the modulation frequency, which implies that part of the radiated or received power is shifted to the sidebands. In order to overcome such a drawback and to improve the performances of the array, the sideband radiation (SR) can be minimized through optimization. Most of the studies on the time-modulation technique are focused on linear antenna arrays, while studies on the time-modulation circular arrays are relatively rare to be seen. Moreover, conventional circular antenna arrays have found many applications in situations where a 360° scan of the main beams are desired, and they play important roles in radio direction finding, radar, sonar, and wireless communication systems, among others (Goto & Tsunoda, 1977; Huang et al., 2009). In addition, antenna arrays with uniform amplitude excitations are easier and less expensive for practical feed network implementation (Yang et al., 2005; Goto & Tsunoda, 1977; Huang et al., 2009; Fondevila et al., 2004). Therefore, with the motivation to overcome the difficult amplitude control problems in a conventional antenna array, a time-modulated circular array (TMCA) with uniform amplitude excitations is utilized to synthesize radiation patterns with prescribed broad nulls in this article. The differential evolution (DE) algorithm is used to optimize the excitation phases and the switch-on time intervals of each element to produce desired wide nulls and suppress the side-lobe levels (SLLs) and the sideband levels (SBLs) simultaneously. A TMCA of 32 identical dipoles with uniform amplitude excitations is considered. Simulation results show that patterns with wide nulls can be achieved successfully, even if the amplitude excitations are uniform.

2. Theoretical Analysis

2.1. TMCA

Consider a circular array of N identical elements equally spaced on the x-y-plane (Figure 1). If a plane wave of frequency f_0 is incident at an angle (θ, φ) with respect to the spherical coordinate system of the array, the output signal from the array is given by

$$E(\theta, \varphi, t) = e^{j2\pi f_0 t} \sum_{k=1}^{N} A_k f_k(\theta, \varphi) e^{j[ka \sin\theta \cos(\varphi - \varphi_k) + \alpha_k]}, \tag{1}$$

where a is the radius of the circular array; A_k and α_k are the static excitation amplitude and phase of the kth element, respectively; and φ_k ($\varphi = 2\pi k/N$) is the angular position of the kth element on the x-y-plane. $f_k(\theta, \varphi)$ is the element pattern of the kth element. To produce an in-phase collimated beam at (θ_0, φ_0), select

$$\alpha_k = -ka \sin\theta_0 \cos(\varphi_0 - \varphi_k). \tag{2}$$

Then the output signal can be rewritten as

$$E(\theta, \varphi, t) = e^{j2\pi f_0 t} \sum_{k=1}^{N} A_k f_k(\theta, \varphi) e^{jka[\sin\theta \cos(\varphi - \varphi_k) - \sin\theta_0 \cos(\varphi_0 - \varphi_k)]}. \tag{3}$$

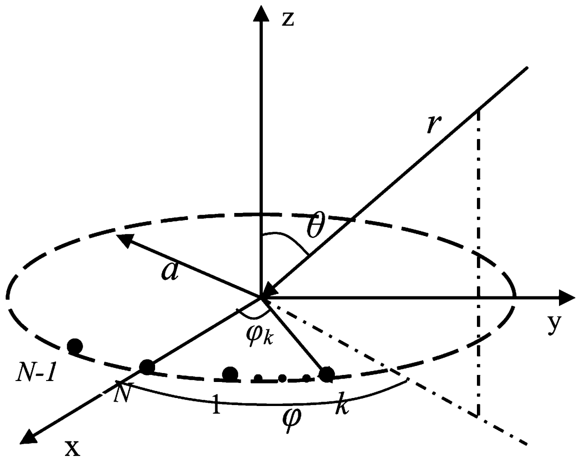

Figure 1. Scheme of an N-element circular array.

Suppose that in the TMCA, each element of the circular array is controlled by a high-speed radio frequency (RF) switch and is excited with a static complex weight $A_k e^{j\alpha_k}$ ($k = 1, 2, \ldots, N$). The periodic switch-on time function $U_k(t)$ ($k = 1, 2, \ldots, N$) (Kummer et al., 1963) for each element can be expressed in the form of

$$U_k(t) = \begin{cases} 1 & 0 \le t \le \tau_k \\ 0 & \text{otherwise} \end{cases}. \tag{4}$$

In Eq. (4), τ_k ($0 \le \tau_k \le T_p$) is the switch-on time of each array element in each modulation period T_p. The time-modulation frequency is $F_p = 1/T_p$. Substituting Eq. (4) into Eq. (1) and decomposing it into a Fourier series with different frequency components $f_0 + m \cdot F_p$ ($m = 0, \pm 1, \pm 2, \ldots, \pm\infty$), the mth-order Fourier component is given by

$$E_m(\theta, \varphi, t) = e^{j2\pi(f_0 + mF_p)t} \sum_{k=1}^{N} A_{mk} f_k(\theta, \varphi) e^{j[ka \sin\theta \cos(\varphi - \varphi_k) + \alpha_k]}. \tag{5}$$

Thus, the radiation patterns of the sideband components ($f_0 + m \cdot F_p$, $m \neq 0$) can be written by Eq. (6):

$$|E_m(\theta, \varphi)| = \left| \sum_{k=1}^{N} A_{mk} f_k(\theta, \varphi) e^{j[ka \sin\theta \cos(\varphi - \varphi_k) + \alpha_k]} \right|. \tag{6}$$

The complex amplitude A_{mk} is given by

$$\begin{aligned} A_{mk} &= \frac{1}{T_p} \int_0^{T_p} \left[A_k \cdot U_k(t) \cdot e^{-j2\pi m F_p t} \right] \cdot dt \\ &= \frac{A_k \cdot \tau_k}{T_p} \cdot \frac{\sin(\pi m \tau_k \cdot F_p)}{\pi m \tau_k \cdot F_p} \cdot e^{-j\pi m \tau_k \cdot F_p}. \end{aligned} \tag{7}$$

At the center frequency f_0 ($m = 0$), the radiation pattern can be specified as

$$|E_0(\theta,\varphi)| = \left| \sum_{k=1}^{N} A_{0k} f_k(\theta,\varphi) e^{j[ka\sin\theta\cos(\varphi-\varphi_k)+\alpha_k]} \right|, \tag{8}$$

$$A_{0k} = A_k \cdot \tau_k / T_p. \tag{9}$$

Therefore, Eq. (9) can be used to synthesize specific patterns at the center frequency f_0. It is known from Eq. (9) that although amplitude excitations are always uniform ($A_k = 1$) throughout this study, the additional variable τ_k can be used to flexibly control the radiation pattern at the center frequency f_0. Thus, the pattern control capability is as good as the amplitude control methods in conventional arrays without the difficulty of implementing a feed network with higher amplitude ratios.

For specific restrictions, assume that the elevation is fixed at 90° and the elements are identical dipoles. The element pattern is $f_k(\theta,\varphi) = \sin\theta$ for each identical dipole. Considering that there are M elements uniformly spaced along the circumference of radius a (where M is assumed to be an even number here) and the symmetric property of the arrays, the excitation amplitude of each element will be $A = 1$, and the phases at the kth, $-k$th, k'th, and $-k'$th elements will be α_k, α_{-k}, $\alpha_{k'}$, $\alpha_{-k'}$, respectively, as shown in Figure 2. Due to the symmetric property of the array, the far-field pattern in the azimuth plane can be simplified into the following form:

$$E(\varphi,t) = 2e^{j2\pi f_0 t} \sum_{k=-N}^{N} A_k \cos\left[ka\cos\left(\varphi + \frac{2k\pi}{M}\right) + \alpha_k\right], \tag{10}$$

where the phases are assumed to be

$$\begin{cases} \alpha_k = \alpha_{-k} = -\alpha_{k'} = -\alpha_{-k'} & \text{for } k = 0,1,2,\ldots,N-1 \\ \alpha_N = \alpha_{-N} = 0 & \text{for } M = 4N \end{cases}. \tag{11}$$

In Eq. (10), $A_k = A$ except that $A_N = A_{-N} = A/2$.

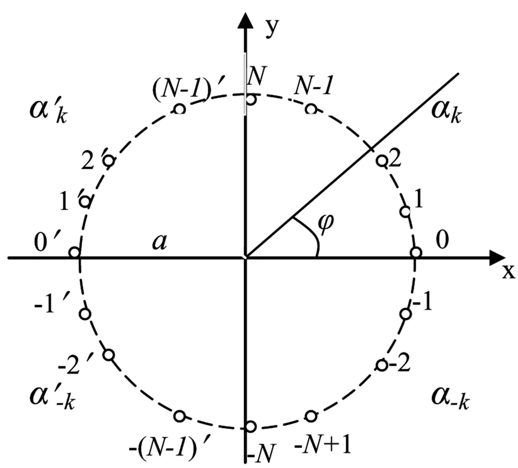

Figure 2. Circular array of $4N$ elements.

The time intervals of each element in the TMCA are assumed to be

$$\begin{cases} \tau_k = \tau_{-k} = \tau_{k'} = \tau_{-k'} & \text{for } k = 1, 2, \ldots, N-1 \\ \tau_0 = \tau_{0'} & \\ \tau_N = \tau_{-N} & \end{cases}. \tag{12}$$

Thus, the radiation pattern of the specific TMCA above would be concretely express as

$$\begin{aligned} E(\varphi, t) &= 2e^{j2\pi f_0 t} \sum_{k=-N}^{N} A_k U_k(t) \cos\left[ka \cos\left(\varphi + \frac{2k\pi}{M}\right) + \alpha_k\right] \\ &= \sum_{m=-\infty}^{\infty} \left\{ 2 \sum_{k=-N}^{N} A_{mk} \cos\left[ka \cos\left(\varphi + \frac{2k\pi}{M}\right) + \alpha_k\right]\right\} \cdot e^{j2\pi(f_0 + mF_p)t}, \end{aligned} \tag{13}$$

where A_{mk} is the same as Eq. (7).

2.2. DE Algorithm

In recent years, many evolutionary optimization algorithms have been successfully applied to the synthesis of arrays patterns (Yang et al., 2002, 2004a; Haupt, 1997; Benedetti et al., 2006; Cutello et al., 2010; Manica et al., 2009; Poli et al., 2010). These optimization techniques, such as the genetic algorithm (GA), simulated annealing (SA) algorithm, particle swarm optimization (PSO) method, and DE algorithm, have been proven to have the ability of finding global minima and can be used to solve various engineering problems. As a global optimization method, the DE algorithm has proved to be an excellent optimizer for various challenging engineering problems, such as electromagnetic inverse scattering (Qing, 2003) and magnetic bearings design (Stumberger et al., 2000). Also, the DE algorithm has been successfully applied to array synthesis problems (Yang et al., 2003, 2005). In many cases of real-valued problems, the DE algorithm outperforms some of the other evolutionary algorithms (Yang et al., 2005; Panduro & Brizuela, 2009). And, it shows better performance in circular antenna arrays as compared with GA and PSO (Panduro & Brizuela, 2009). Therefore, the DE algorithm was chosen to optimize the phases and the switch-on time intervals of each element in this article. The main optimization procedure of the DE algorithm is introduced briefly in what follows.

The DE algorithm operates on a population of *NP* candidate solutions $X_{i,G}$ ($i = 1, \ldots, NP$), where the index i denotes the population and G denotes the generation to which the population belongs. It follows a general procedure of an evolutionary algorithm using the three kinds of operators: mutation, crossover, and selection; however, these are quite different from those in the GA.

The DE algorithm starts by initializing the population randomly to cover the entire space uniformly. It differs from the GA in that the mutation operator takes place first, and the process at each generation begins by randomly selecting three individuals $\{r_1, r_2, r_3\}$ in the population set of *NP* elements. The ith perturbed individual $V_{i,G+1}$ can be generated according to

$$V_{i,G+1} = X_{r_3,G} + F * (X_{r_1,G} - X_{r_2,G}), \tag{14}$$

where $i = 1, \ldots, NP$, $r_1, r_2, r_3 \in \{1, \ldots, NP\}$ are randomly selected such that $r_1 \neq r_2 \neq r_3 \neq i$; F is the control parameter (mutation factor) such that $F \in [0, 1]$. The mutation applies the vector differentials between the existing population members for determining the perturbation of the individual. This process can avoid the harmful mutation exist in the GA.

Then the perturbed individual $V_{i,G+1} = (v_{1,i,G+1}, \ldots, v_{n,i,G+1})$ and the current population member $X_{i,G} = (x_{1,i,G}, \ldots, x_{n,i,G})$ are subject to the crossover operation, which finally generates the population of candidates (child vectors) $U_{i,G+1} = (u_{1,i,G+1}, \ldots, u_{n,i,G+1})$ according to

$$u_{j,i,G+1} = \begin{cases} v_{j,i,G+1} & \text{if } rand_j \leq C_r \vee j = k \\ x_{j,i,G} & \text{otherwise} \end{cases}, \tag{15}$$

where $j = 1, \ldots, n$; $k \in \{1, \ldots, n\}$ is a random parameter's index; and $rand_j$ is a real random number in the range [0, 1]. The crossover factor $C_r \in [0, 1]$ is set by the Suser.

Finally, the selection operation takes place. The population for the next generation is selected from the individual in the current population and its corresponding trial vector according to the following rule:

$$X_{i,G+1} = \begin{cases} U_{i,G+1} & \text{if } f(U_{i,G+1}) \leq f(X_{i,G}) \\ X_{i,G} & \text{otherwise} \end{cases}. \tag{16}$$

The fitness value of the child vector is compared with its corresponding parent vector, and the one with the lower objective function value will survive from the tournament selection to the population of the next generation. In this way, all the individuals of the next generation are as good as or better than their counterparts in the current generation. The overall procedure repeats until the maximum number of generation are used up or the prefixed iteration accuracy is achieved.

The proper choice of the parameters (F, C_r, NP) and the objective function is crucial to the convergence of the minimization problem. The initialized population should be spread as much as possible over the objective function surface, and for many applications, $NP = 10*D$ is a good choice, where D is the dimension of the vector $X_{i,G}$ or the number of the optimized variable (Storn & Siemens AG, 1996). However, in some applications (Huang et al., 2009; Yang et al., 2004a), it is effective to set $NP = 5 * D$ to speed up the convergence rate. The crossover factors F and C_r are usually chosen as $\in [0.5, 1]$ and $[0.8, 1]$, respectively. The specific parameter value is set by the user for different conditions.

In this article, the vector $X_{i,G} = \{\tau_k, \alpha_k\}$ is defined to indicate all the parameters to be optimized. Meanwhile, the SRs $(m \neq 0)$ are considered to be suppressed to improve the radiation efficiency (Bregains et al., 2008; Poli et al., 2010; Yang et al., 2002). Thus, in order to place broad nulls in the desired direction as well as suppress the SLLs and the SBL, the objective function is constructed as

$$f^{(n)}(v) = \sum_{i=1}^{M} w_i \left| E_i^{(n)}(v) - NLD_i \right| + w_{M+1} \cdot SLL_{\max}^{(n)}(v) \left|_{f_0} + w_{M+2} \cdot SBL_{\max}^{(n)}(v) \right|_{f_0+F_p}, \tag{17}$$

where n represents the number of evolution generations, M stands for the total number of the specified angles of interference sources at interval of 1°, NLD_i is the desired null depth level for the ith interference source, $SLL_{\max}$ and $SBL_{\max}$ are the maximum SLL at the center frequency and the maximum SBL at the first sideband frequency, respectively. And w_i ($i = 1, 2, \ldots, M + 2$) are the weighting factors of each term to emphasize the different contributions to the cost function. The weighing factors are continuously adjusted until the minimization is going to converge.

3. Numerical Results and Discussion

In order to show the capabilities of setting wide nulls in the direction of the interference region by applying the time-modulation technique into circular antenna arrays, a TMCA of 32 identical dipoles with uniform amplitude excitations is modeled (where $M = 32$, $N = 8$ as shown in Figure 2); some numerical results are presented in this section. In this study, the typical DE simulation parameters (Yang et al., 2004a) are set as follows: $NP = 5 * D$, $F = 0.6$, and $C_r = 0.9$. The search ranges of the excitation phases α_k (in radians) are selected as $[-\pi, \pi]$, and the normalized switch-on time intervals τ_k are selected as [0.06, 1.0], which is determined by the minimum operating time step of the high-speed RF switch.

3.1. Example 1

For the first example, a TMCA of 32 identical dipoles, which are equally spaced at half a wavelength apart along the circumference (where $ka = N/2 = 16$), is considered. The element pattern of the dipole is selected to be $\sin\theta$. Owing to the array symmetry, there are only 17 parameters (the zeroth, first, second, ..., seventh elements phases and the zeroth, first, second, ..., eighth normalized switch-on time intervals) to be optimized. As can be seen from Figures 3 and 4, the normalized radiation patterns with a prescribed wide null in the range of [50°, 70°] and [80°, 130°] are successfully synthesized. It is shown in Figure 3(a) that the SLL is −25 dB and the null depth is −56.8 dB, where the null depth is 7.8 dB lower than that of the conventional array in (Lu & Yeo, 2000). In addition, as shown in Figure 3(a), an additional wide null region is also placed in the symmetric direction of [−70°, −50°]. Also, it can be seen from Figure 4(a) that the SLL is −25 dB and the null depth is −58.7 dB in the band [80°, 130°] as well as the symmetric band [−130°, −80°], where the null depth is 8.7 dB lower than the result in Lu and Yeo (2000). As stated by Haupt (1997), nulling interference sources at symmetric angles about the main beam is difficult for phase-only nulling, but it is convenient to set symmetric nulls in the TMCA. As shown in Figures 3(b) and 4(b), the maximum SBLs were suppressed to −15 dB, which means that the electromagnetic energy shifted to sidebands are relatively small. Numerical results show the achievable performance of the approach in successfully synthesizing patterns with desirable broad nulls, even if the amplitude excitations are uniform. The only defect is that the 3-dB beamwidth is wider than that of Lu and Yeo (2000), and this is due to the fact that the additional wide null placed in the symmetric angle position and the arrays are uniformly excited. However, it still has an advantage in the case of the interference signal distributing on both sides of the main lobe. The excitation phases and normalized switch-on time intervals of the elements numbered $0, 1, \ldots, 7$, and 8 for the two far-field patterns of different null bands in the first example are shown in Table 1, and the excitations of other elements can be readily obtained through Eqs. (11) and (12).

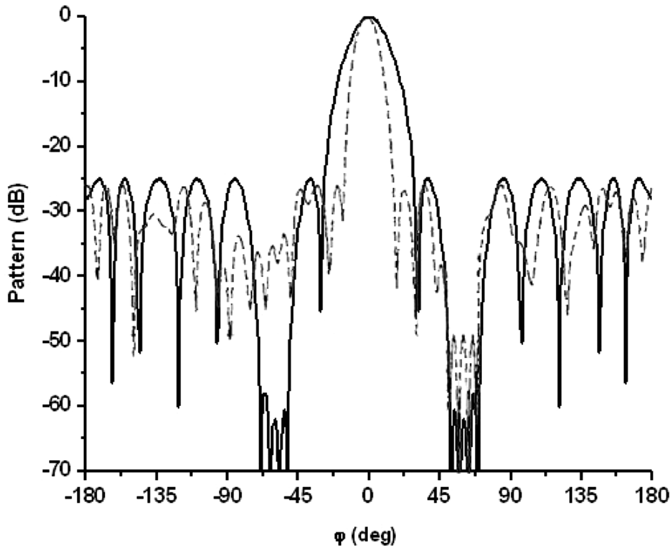

(a)

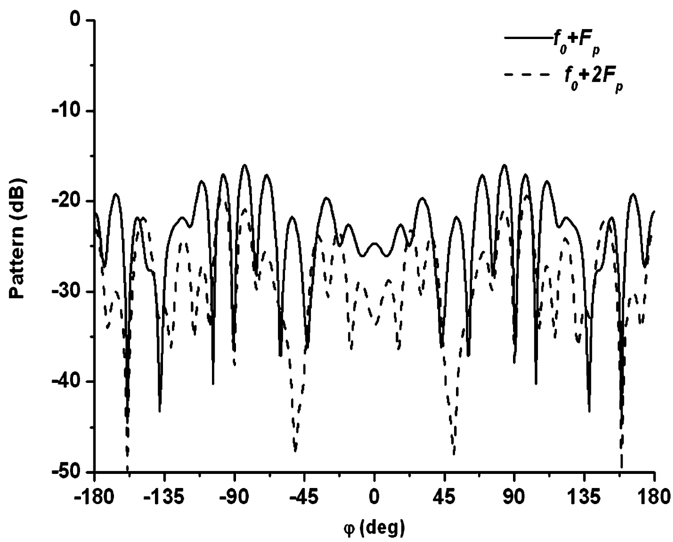

(b)

Figure 3. Normalized radiation patterns of the $\lambda/2$-spaced 32-element TMCA with nulls in the range of $[-70°, -50°]$ and $[50°, 70°]$ ($ka = 16$): (a) solid line: pattern synthesized in this article at f_0; dashed line: pattern synthesized by Lu et al. (2000) and (b) corresponding sideband patterns at $f_0 + F_p$ and $f_0 + 2F_p$.

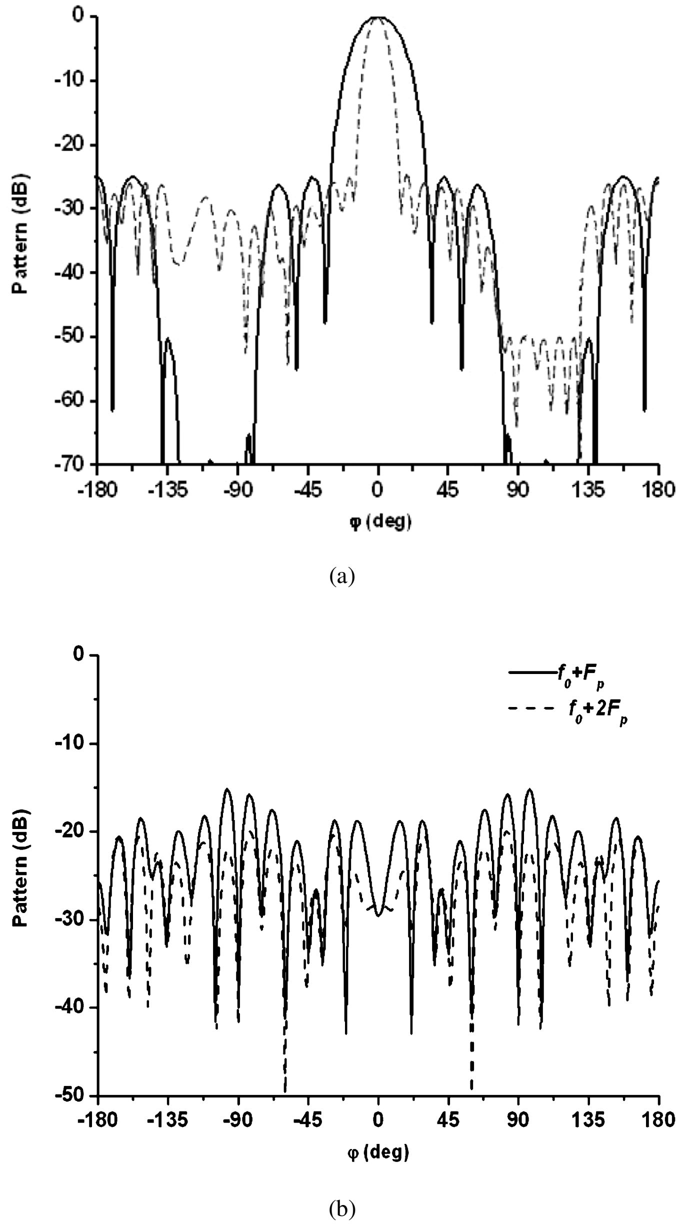

Figure 4. Normalized radiation patterns of the $\lambda/2$-spaced 32-element TMCA with nulls in the range of $[-130°, -80°]$ and $[80°, 130°]$ ($ka = 16$): (a) solid line: pattern synthesized in this article at f_0; dashed line: pattern synthesized by Lu et al. (2000) and (b) corresponding sideband patterns at $f_0 + F_p$ and $f_0 + 2F_p$.

Table 1

Excitation phases and normalized switch-on time intervals of the $\lambda/2$-spaced 32-element TMCA ($ka = 16$) (Case 1—nulls in the range of $[-70°, -50°]$ and $[50°, 70°]$; Case 2—nulls the range of $[-130°, -80°]$ and $[80°, 130°]$)

	8	7	6	5	4	3	2	1	0
Case 1 (k)									
α_k (rad.)	0.0000	−1.5789	−1.6879	−1.5071	−0.7417	1.6348	1.5191	1.1128	0.8383
τ_k (μs)	0.0600	0.6264	0.9258	0.7175	0.1216	0.6426	0.9999	1.0000	1.0000
Case 2 (k)									
α_k (rad.)	0.0000	1.5670	1.6676	1.6031	−0.7022	−1.6373	−1.8241	−2.0772	−2.2284
τ_k (μs)	0.0600	0.6867	0.9489	0.6618	0.0667	0.7207	0.9999	0.9619	0.9278

3.2. *Example 2*

The second example considers the same TMCA, except the element space was changed from half a wavelength into a quarter wavelength (where $ka = 8$). Figures 5 through 7 depict the normalized power patterns with variable null width and depth of the TMCA in the range of $[-50°, -30°]$ and $[30°, 50°]$, $[-80°, -50°]$ and $[50°, 80°]$, and $[-140°, -80°]$ and $[80°, 140°]$, respectively. It is noted that the SLLs are −26, −26.3, and −26.7 dB, respectively, which are relatively lower than the −25 dB SLL in Lu and Yeo (2000). Also from Figures 5 through 7, it is seen that the null depths are below −54.6, −55.8, and −54.6 dB for each null region. While in Lu and Yeo (2000), the null depth is −49 dB for 20° null width in the band $[50°, 70°]$ and −50 dB for 50° null width in the band $[80°, 130°]$. Thus, the performance of the null width and depth has been improved as compared to the results of Lu and Yeo (2000). Moreover, the SBLs of the three patterns were further suppressed to below −20 dB, which is a sufficiently small SBL for the

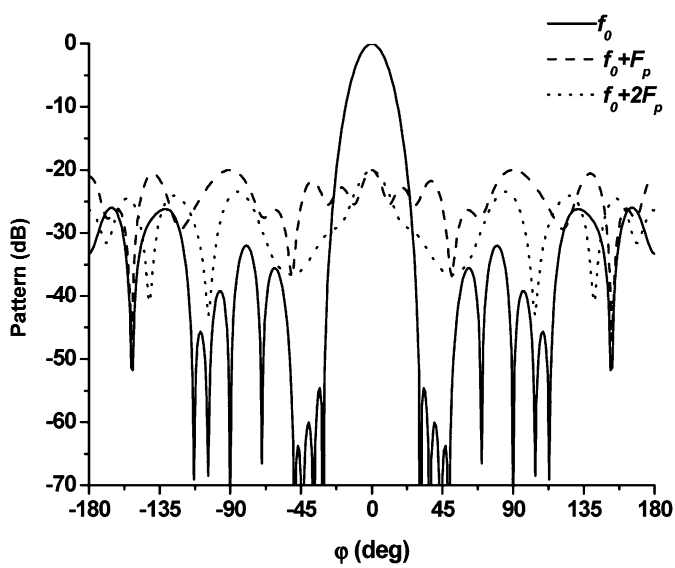

Figure 5. Normalized radiation patterns of the $\lambda/4$-spaced 32-element TMCA with nulls in the range of $[-50°, -30°]$ and $[30°, 50°]$ ($ka = 8$).

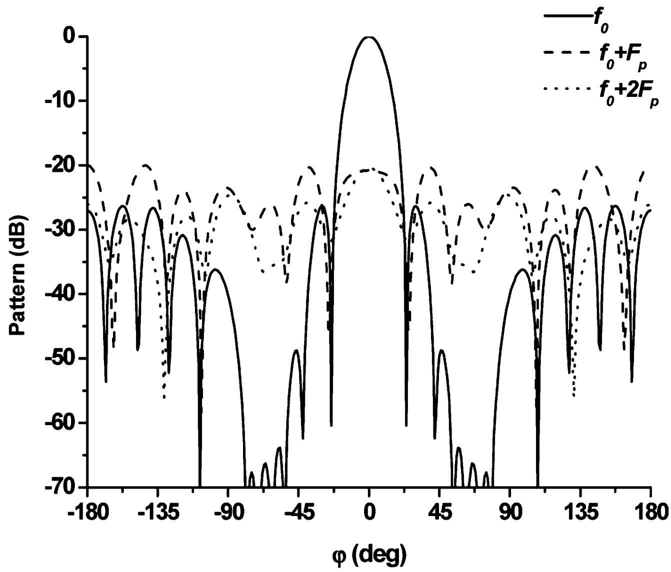

Figure 6. Normalized radiation patterns of the $\lambda/4$-spaced 32-element TMCA with nulls in the range of $[-80°, -50°]$ and $[50°, 80°]$ $(ka = 8)$.

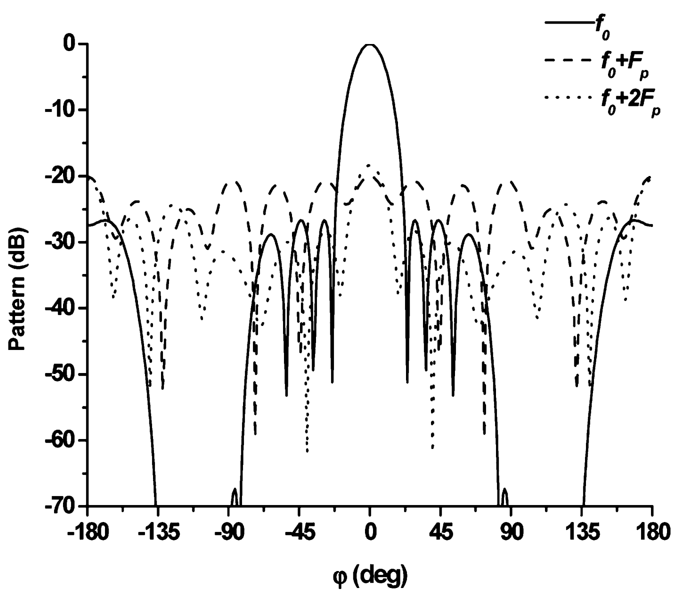

Figure 7. Normalized radiation patterns of the $\lambda/4$-spaced 32-element TMCA with nulls in the range of $[-140°, -80°]$ and $[80°, 140°]$ $(ka = 8)$.

reduction of the inherent power loss due to time modulation. Furthermore, it shows that the null width, SLL, SBL, and the 3-dB beamwidth have been improved to acquire better results as compared to the first example. In general, it shows the flexibility of this simple approach by only adjusting the phase of the array and the switch-on time interval without changing the amplitude excitations.

4. Conclusion

This article presents an approach of pattern synthesis with specified variable wide nulls in the side-lobe region. The uniform amplitude TMCA is adopted, and the desired radiation patterns with specific restrictions are successfully synthesized. Numerical results show that by using the time-modulation technique, the excellent pattern control capability in amplitude-phase methods is retained, while the difficulty of the higher amplitude ratios in the amplitude control technique is eliminated. The null width can be up to 60°, which is essentially difficult for conventional antenna arrays. The proposed approach can be used to effectively suppress the interference signals incident from several different directions within a certain angle range or varying slightly with time.

Acknowledgments

This work was supported in part by the Natural Science Foundation of China (grant 60971030) and in part by the 111 Project of China (grant B07046).

References

Benedetti, M., R. Azaro, D. Franceschini, & A. Massa. 2006. PSO-Based real-time control of planar uniform circular arrays. *IEEE Antenna Wireless Propagat. Lett.* 5:843–846.

Bregains, J. C., J. Fondevila-Gomez, G. Franceschetti, & F. Ares. 2008. Signal radiation and power losses of time-modulated arrays. *IEEE Trans. Antennas Propagat.* 56:1799–1804.

Cutello, V., G. Nicosia, M. Pavone, & G. Stracquadanio. 2010. Entropic divergence for population based optimization algorithm. *IEEE Congress on Evolutionary Computation (CEC)*, Barcelona, Spain, 18–23 July.

Er, M. H. 1988. Technique for antenna array pattern synthesis with controlled broad nulls. *IEE Microw. Antennas Propagat.* 135:375–380.

Er, M. H. 1990. Linear antenna array pattern synthesis with prescribed broad nulls. *IEEE Trans. Antennas Propagat.* 38:1496–1498.

Fondevila, J., J. C. Brégains, F. Ares, & E. Moreno. 2004. Optimizing uniformly excited linear arrays through time modulation. *IEEE Antennas Wireless Propagat. Lett.* 3:298–301.

Gething, P. J. D., & J. B. Haseler. 1974. Linear antenna arrays with broadened nulls. *Proc. Institut. Elect. Eng.* 121:165–168.

Giusto, R., & P. De Vincenti. 1983. Phase-only optimization for the generation of wide deterministic nulls in the radiation pattern of phased arrays. *IEEE Trans. Antennas Propagat.* 31:814–817.

Gome-Tomero, J. L., A. J. Martinez-Ros, & R. Verdu-Monedero. 2010. FFT synthesis of radiation patterns with wide nulls using tapered leaky-wave antennas. *IEEE Antennas Wireless Propagat. Lett.* 9:518–521.

Goto, N., & Y. Tsunoda. 1977. Sidelobe reduction of circular arrays with a constant excitation amplitude. *IEEE Trans. Antennas Propagat.* 25:896–898.

Guney, K., & M. Onay. 2007. Amplitude-only pattern nulling of linear antenna with the use of bees algorithm. *Progr. Electromagn. Res.* 70:21–36.

Haupt, R. L. 1997. Phase-only adaptive nulling with a genetic algorithm. *IEEE Trans. Antennas Propagat.* 45:1009–1015.

Huang, M., S. Yang, G. Li, & Z. Nie. 2009. Synthesis of low and equal-ripple sidelobe patterns in time-modulated circular array antennas. *J. Infrared Millim. Terahertz Waves* 30:802–812.

Karaminas, P. D., & A. Manikas. 2000. Super-resolution broad null beamforming for cochannel interference cancellation in mobile radio networks. *IEEE Trans. Vehicular Technol.* 49:689–697.

Kummer, W. H., A. T. Villeneuve, T. S. Fong, & F. G. Terrio. 1963. Ultra-low sidelobes from time-modulated arrays. *IEEE Trans. Antennas Propagat.* 11:633–639.

Lu, Y., & B.-K. Yeo. 2000. Adaptive wide null steering for digital beamforming array with the complex coded genetic algorithm. *IEEE International Conference on Phased Array Systems and Technology*, Dana Point, CA, 21–25 May, 557–560.

Manica, L., P. Rocca, L. Poli, & A. Massa. 2009. Almost time-independent performance in time-modulated linear arrays. *IEEE Antenna Wireless Propagat. Lett.* 8:843–846.

Panduro, M. A., & C. A. Brizuela. 2009. A comparative analysis of the performance of GA, PSO and DE for circular antenna arrays. *IEEE Antenna and Propagation Society International Symposium*, 1–5 June, 1–4.

Poli, L., Rocca, P., L. Manica, & A. Massa. 2010. Handling sideband radiations in time-modulated arrays through particle swarm optimization. *IEEE Trans. Antennas Propagat.* 58:1408–1400.

Qing, A. 2003. Electromagnetic inverse scattering of multiple two-dimensional perfectly conducting objects by the differential evolution strategy. *IEEE Trans. Antennas Propagat.* 51:1251–1262.

Rocca, P., L. Manica, L. Poli, & A. Massa. 2009. Synthesis of compromise sum-difference arrays through time-modulation. *IET Radar Sonar Navigat.* 3:630–637.

Rocca, P., L. Poli, G. Oliveri, & A. Massa. 2010. Synthesis of time-modulated planar arrays with controlled harmonic radiations. *J. Electromagn. Waves Appl.* 24:827–838.

Storn, R., & M. Siemens AG. 1996. On the usage of differential evolution for function optimization. *Biennial Conference of the North American Fuzzy Information Processing Society (NAFIPS)*, Berkeley, CA, 19–22 June, 519–523.

Stumberger, G., D. Dolinar, U. Palmer, & K. Hameyer. 2000. Optimization of radial active magnetic bearings using the finite element technique and the differential evolution algorithm. *IEEE Trans. Magn.* 36:1009–1013.

Yang, S., Y. Chen, & Z. Nie. 2009. Simulation of time modulated linear antenna arrays using the FDTD method. *Progr. Electromagn. Res.* 98:175–190.

Yang, S., Y. B. Gan, & A. Qing. 2002. Sideband suppression in time-modulated linear arrays by the differential evolution algorithm. *IEEE Antennas Wireless Propagat. Lett.* 1:173–175.

Yang, S., Y. B. Gan, & A. Qing. 2004a. Antenna array pattern nulling using a differential evolution algorithm. *Int. J. RF Microw. Comput.-Aided Eng.* 14:57–63.

Yang, S., Y. B. Gan, A. Qing, & P. K. Tan. 2005. Design of a uniform amplitude time modulated linear array with optimized time sequences. *IEEE Trans. Antennas Propagat.* 53:2337–2339.

Yang, S., Y. B. Gan, & P. K. Tan. 2003. A new technique for power-pattern synthesis in time-modulated linear arrays. *IEEE Antennas Wireless Propagat. Lett.* 2:285–287.

Yang, S., Y. B. Gan, & P. K. Tan. 2004b. Comparative study of low sidelobe time modulated linear arrays with different time schemes. *J. Electromagn. Waves Appl.* 18:1443–1458.